Original Article

DOI: 10.5582/bst.2024.01096

Ligustrazine alleviates the progression of coronary artery calcification by inhibiting caspase-3/GSDME mediated pyroptosis

Honghui Yang*, Guian Xu, Qingman Li, Lijie Zhu

Department of Cardiology, Zhengzhou University, Central China Fuwai Hospital, Zhengzhou, China.

SUMMARY Coronary artery calcification (CAC) is an early marker for atherosclerosis and is mainly induced by the osteoblast-like phenotype conversion of vascular smooth muscle cells (VSMCs). Recent reports indicate that NOD-like receptor protein 3 (NLRP3)-mediated pyroptosis plays a significant role in the calcification of vascular smooth muscle cells (VSMCs), making it a promising target for treating calcific aortic valve disease (CAC). Ligustrazine, or tetramethylpyrazine (TMP), has been found effective in various cardiovascular and cerebrovascular diseases and is suggested to inhibit NLRP3-mediated pyroptosis. However, the function of TMP in CAC is unknown. Herein, influences of TMP on β-glycerophosphate (β-GP)-stimulated VSMCs and $OPG^{-/-}$ mice were explored. Mouse Aortic Vascular Smooth Muscle (MOVAS-1) cells were stimulated by β-GP with si- caspase-3, si- Gasdermin E (GSDME) or TMP. Increased calcification, reactive oxygen species (ROS) level, Interleukin-1beta (IL-1β) and Interleukin-18 (IL-18) levels, lactate dehydrogenase (LDH) release, enhanced apoptosis, and activated cysteine-aspartic acid protease-3 (caspase-3)/GSDME signaling were observed in β-GP-stimulated MOVAS-1 cells, which was sharply alleviated by si-caspase-3, si-GSDME or TMP. Furthermore, the impact of TMP on the β-GP-induced calcification and injury in MOVAS-1 cells was abolished by raptinal, an activator of caspase-3. Subsequently, $OPG^{-/-}$ mice were dosed with TMP or TMP combined with raptinal. Calcium deposition, increased nodules, elevated IL-1β and IL-18 levels, upregulated CASP3 and actin alpha 2, smooth muscle (ACTA2), and activated caspase-3/GSDME signaling in $OPG^{-/-}$ mice were markedly alleviated by TMP, which were notably reversed by the co-administration of raptinal. Collectively, TMP mitigated CAC by inhibiting caspase-3/GSDME mediated pyroptosis.

Keywords coronary artery calcification, Ligustrazine, caspase-3, GSDME, vascular smooth muscle cells

1. Introduction

Cardiovascular disease ranks first in morbidity and mortality in the world, which is one of the most common chronic diseases and one of the most susceptible diseases in the elderly. Despite advances in the diagnosis and treatment of cardiovascular disease, the incidence is still increasing (*1*). CAC is an important marker of the late development of coronary atherosclerosis (CAS). CAC is a common type of arterial calcification, which contributes to the reduction of coronary vessel compliance. Abnormal vasoconstrictor response and impaired myocardial perfusion are risk factors for poor prognosis in patients with revascularization and coronary heart diseases (*2,3*). The degree of CAC has a certain impact on the stability of plaque. For example, microcalcifications within the fibrous cap may lead to plaque rupture (*4*), while the fibrous cap will be disrupted by calcified nodules to expose collagen fibers and induce thrombosis (*5*). In addition, recurrent plaque rupture and healing after hemorrhage may lead to the development of obstructive fibrocalcific lesions, causing the occurrence of angina and sudden death (*6*). Currently, no effective agents for treating CAC are available in the clinic. Several reported treatment strategies, such as statins and RAAS system inhibitors, are reported with non-ideal results (*7*), and some studies even show that statins aggravate the development of calcification (*8*). As the pathogenesis of CAC is complex and the clinical therapeutic methods are lacking, studying the pathogenesis of vascular calcification and developing novel therapeutic drugs are of great significance.

VSMCs are contractile cells located in the vascular wall, and secrete pro-or anti-calcification factors. The osteoblast-like phenotype conversion of VSMCs is claimed to be the most important inducer in vascular

calcification. Following the stimulation of factors, such as oxidative stress, inflammation, calcium and phosphorus internal environment disorders, the phenotype conversion of VSMCs to osteoblast-like cells is induced. By secreting bone-related transcription factors and upregulating bone-related proteins, osteoblasts promote the formation of vascular calcification (*9*). Matrix vesicles will be released by apoptotic VSMCs or osteoblast-like cells. These matrix vesicles are rich in phospholipids and convert calcium ions to amorphous calcium phosphate, which is further converted to hydroxyapatite. The process of calcification starts on the surface of the vesicle or inside the vesicle, and contributes to the initiation of calcification (*10*). Recently, the role of NLRP3-mediated pyroptosis in the calcification of VSMCs has been widely reported (*11,12*). Regulating the pyroptosis of VSMCs will be a promising method for treating CAC.

In 2017, Wang *et al.* (*13*) reported that Gasdermin E (GSDME), a member of the Gasdermin protein family, can be cleaved by caspase-3 and mediates development of pyroptosis, which is consistent with the results of Shao Feng's team (*14*) in the same year. GSDME and GSDMD belong to the Gasdermin family and share a pore forming structure (*15*). Unlike GSDMD, cleavage of GSDME does not involve caspase-1 or caspase-4/5/11 pathways. Instead, GSDME relies on caspase-3, another member of the caspase protein family. In contrast to other members of the caspase protein family, caspase-3 is located at the end of the caspase cascade and is a major effector enzyme. Upon activation by upstream caspases, caspase-3 is involved in the execution of apoptosis and the activation of other inflammatory mediators (*16,17*).

The research team at Amgen in the United States first found OPG in the cDNA library of rat small intestine in 1997 (*18*). In the same year, Tsuda *et al.* also found a cytokine that could inhibit the formation of osteoclasts in the culture medium of human embryonic fibroblasts, which was named as osteoclast formation inhibitory factor (OCIF) (*19*). In subsequent studies, Ten *et al.* inferred and analyzed the amino acid sequences of OPG and OCIF, and finally confirmed that OCIF and OPG were the same protein (*20*). It is widely reported that the OPG/RANKL/RANK system participates in vascular calcification. Price *et al.* found that in the mouse model of vascular calcification established by the induction of warfarin and toxic doses of VitD, supplementation of OPG significantly inhibited progression of vascular calcification (*21*). The $OPG^{-/-}$ mice established by Bucay developed progressively aggravated systemic osteoporosis after birth, accompanied by medial calcification of the aorta and/or renal artery (*22*). Min *et al.* confirmed that intravenous injection of recombinant OPG protein or transgenic overexpression of OPG inhibited occurrence of vascular calcification and osteoporosis in $OPG^{-/-}$ mice (*23*). These data indicate that OPG is associated with osteoporosis and vascular calcification, and is a protective factor for vascular calcification. The $OPG^{-/-}$ mouse is a recognized animal model of arterial calcification and has incomparable advantages in studying the role of the OPG/RANKL/RANK system in arterial calcification (*24*).

Ligustrazine, also named as 2, 3, 5, 6-tetramethylpyrazine (TMP), mainly extracted from the root of Chuanxiong rhizoma, is a non-volatile alkaloid with anti-ischemia-reperfusion injury and protective effects against cell damage, which provides a foundation for the clinical application of TMP in the treatment of various cardiovascular and cerebrovascular diseases (*25*). Furthermore, TMP is reported to have promising antioxidant effects (*26*). The previous study has confirmed the therapeutic function of TMP against atherosclerosis (*27*). Moreover, several reports have claimed the inhibitory effect of TMP on NLRP3-mediated pyroptosis (*28,29*). However, the potential therapeutic function of TMP against CAC remains uncertain. Herein, the regulatory effect of TMP on β-GP-treated VSMCs and $OPG^{-/-}$ mice was explored.

2. Materials and Methods

2.1. Cells and treatments

Mouse vascular smooth muscle cell line, MOVAS-1 cells, was obtained from ATCC (USA) and cultured in DMEM medium involving penicillin/streptomycin and 10% FBS at 5% CO2 and 37°C. To establish the *in vitro* vascular calcification model, MOVAS-1 cells were treated with 2.5 mM β-glycerophosphate (β-GP, Sigma, UK) for 21 days.

2.2. Transfection

To knockdown the caspase-3 and GSDME level in MOVAS-1 cells, cells were transfected with the siRNA targeting caspase-3 (si-caspase-3) and the siRNA targeting GSDME (si-GSDME) with lipofectamine3000 (Thermo Fisher, USA). Si-NC was used as a negative control for siRNAs. After culturing lipofectamine3000 and siRNAs separately in serum-free medium for 5 min, 2 solutions were mixed and incubated for 20 min, followed by being introduced into MOVAS-1 cells and incubating for 48 h. All siRNAs were synthesized by Genscript (Nanjing, China). Sequences of siRNAs are shown in Table 1.

2.3. RT-PCR

MOVAS-1 cells were collected to extract total RNAs using the TrizoI reagent (15596026, Invitrogen, USA). Subsequently, cDNA synthesis was performed utilizing the RT-PCR reverse transcription kit (205311, QIAGEN, USA), followed by PCR amplification in the PCR instrument (Quant Studio5, Thermo Fisher, USA). The

Table 1. Sequences of siRNAs

SiRNAs	Sense (5'-3')	Antisense (5'-3')
Si-GSDME	GGAUCAGGAUCUAUUACCUTT	AGGUAAUAGAUCCUGAUCCTT
Si-caspase-3	TGACATCTCGGTCTGGTAC	TACCAGTGGAGGCCGACTT
Si-NC	CCAAGAACTTCCAGAACATAT	ATATGTTCTGGAAGTTCTTGG

internal reference gene was GAPDH and gene levels were determined utilizing the $2^{-\Delta\Delta Ct}$ method.

2.4. Alizarin red staining

After fixing with 4% paraformaldehyde for 10 min, MOVAS-1 cells were stained with alizarin red solution (2003999, Sigma, USA) in the dark for half an hour. Then, cells were washed with ddH2O 3 times, followed by observation under the optical microscope (SP8, Leica, Germany).

2.5. ROS detection using the flow cytometry

MOVAS-1 cells were centrifuged at 300 g for 10 min and collected, followed by resuspension using serum-free medium containing 10 μM DCFH-DA. After incubating at 37 °C for 20 min, cells were rinsed with PBS and loaded onto flow cytometry (CytoFLEX3, Beckman, USA) to detect the ROS level.

2.6. The detection of LDH release

After plating on 96-well plates, MOVAS-1 cells were exposed to LDH reagent (11644793001, Sigma, USA), followed by 90 min incubation in the dark. Then, the optical density was determined utilizing a microplate reader (EnSpire, PerkinElmer, USA) at 490 nm, followed by calculating LDH release according to the standard curve.

2.7. ELISA assay for cytokine level detection

The IL-1β (E-EL-M0037c, eBioScience, USA) and IL-18 level (BMS618-3, eBioScience, USA) were detected using commercial kits. The coronary artery tissues were collected and homogenized, followed by centrifugation and collecting the supernatant. For cell samples, MOVAS-1 cells were centrifuged at 300 g for 10 min and supernatant was collected. 50 μL supernatant was diluted to a 1:1 ratio, which was loaded into the wells. Then, 50 μL Biotin-labeled antibody was introduced and cultured for 60 min at 37°C, followed by removing the reagent and adding 80 μL HRP-loaded secondary antibody. Following half an hour culture at 37°C, 50 μL TMB substrates were added and cultured at 37°C for 10 min, followed by loading 50 μL stop solution. Lastly, the OD value was measured utilizing a microplate reader (EnSpire, PerkinElmer, USA).

2.8. Hoechst/PI staining

MOVAS-1 cells were loaded into 6-well plates and cultured overnight, followed by discarding the medium and introducing 10 μL Heochst staining reagent at 37°C in the dark for 12 min. Cells were then centrifuged at 300 g at 4°C for 5 min and the medium was discarded, followed by introducing 5 μL PI solution and placement in the dark for 6 min. 50 μL stained cells were dropped onto a cover glass and observed under the fluorescence microscope (DM2500, Leica, Germany).

2.9. Animals and grouping

Thirty male $OPG^{-/-}$ mice (7-9 weeks, 18-22 g) and 12 male wide type mice (WT, 7-9 weeks, 18-22 g) were purchased from Shanghai Model Organisms Center, Inc (China) and raised in the SPF laboratory with controlled humidity, temperature and a 12/12 light/dark cycle. After 1-week of adaption, animals were divided into 3 groups (n=6/group): Control, Model, and TMP. In the Model and TMP groups, $OPG^{-/-}$ mice were orally administered 200 μL/day normal saline and 80 mg/kg/day TMP for 4 weeks. In the control group, WT mice were orally administered 200 μL/day normal saline for 4 weeks. To verify the potential mechanism of TMP in calcification, animals were divided into 4 groups (n=6/group): Control, Model, TMP, and TMP+raptinal. Administrations of the control, model, and TMP groups are listed above. In the TMP+raptinal group, $OPG^{-/-}$ mice were orally administered 80 mg/kg/day TMP for 4 weeks and 20 mg/kg/day raptinal for 3 consecutive days in the beginning.

All animal experiments were authorized by the ethics committee of Central China Fuwai Hospital, Zhengzhou University (No.2021032).

2.10. HE staining assay

Coronary artery tissues were fixed in 4% paraformaldehyde solution for 90 min, dehydrated in a gradient of 70% to 100% ethanol, transparent in xylene, embedded in paraffin, and sectioned. Paraffin sections were deparaffinized with xylene and eluted in xylene for 10 min, 100% ethanol for 5 min, 90% ethanol for 5 min, 80% ethanol for 5 min, 70% ethanol for 5 min, and distilled water for 5 min, followed by staining with hematoxylin for 10 min, washed with distilled water for 10 min, differentiated in 1% hydrochloric acid for several seconds, and counterstained with eosin. Slices

were dehydrated, dried, and sealed with neutral gum, and observed under a microscope (SP8, Leica, Germany).

2.11. Von Kossa staining assay

After deparaffinization and dehydration, sections were exposed to nitrate solution for 30 min for staining. After washing with distilled water three times, sections were fixed with sodium thiosulfate solution and counterstained with neutral fuchsin. Calcium deposition was observed under a microscope (SP8, Leica, Germany) after rinsing again with distilled water.

2.12. Western blotting assay

Coronary artery tissues or MOVAS-1 cells were collected to extract total proteins using the RIPA lysis buffer, followed by quantification with the BCA method (23227, Elabscience, USA). The separation of proteins was conducted using SDS-PAGE, followed by transferring the separated proteins onto a PVDF membrane. Blocking was conducted using 5% skim milk and primary antibodies against pro-caspase-3 (1/1000, ab32150, Abcam, USA), cleaved-caspase-3 (1/500, ab32042, Abcam, USA), GSDME-N (1:1000, ab215191, Abcam, USA), NLRP3 (1:1000, ab263899, Abcam, USA), and GAPDH (1:2000, ab8245, Abcam, USA). Subsequently, the secondary antibody (1:4000, ab288151, Abcam, USA) was introduced and cultured for 60 min. ECL solution was loaded for exposure and the protein level was quantified with Image J software.

2.13. Immunofluorescence assay

Sections of coronary artery tissues were rinsed utilizing distilled water and incubated using 10% goat serum for blocking, followed by introducing the primary antibody against CASP3 (1:25, ab32351, Abcam, USA) and ACTA2 (1:25, ab7817, Abcam, USA) overnight at 4°C. After washing several times, sections were incubated with secondary antibody (1:200, ab150077, Abcam, USA) for 90 min at 37°C and then stained with DAB dye, followed by observing the images using the fluorescence microscope (DM2500, Leica, Germany).

2.14. Statistical analysis

Data was expressed as Mean ± SD. The comparison among three or more groups was analyzed using the one-way ANOVA (Tukey's method). The analysis was conducted using GraphPad software (GraphPad Prism 8) and $p < 0.05$ was taken as a significant difference.

3. Results

3.1. Caspase-3/GSDME axis participated in β-GP-induced calcification in MOVAS-1 cells

To explore the function of the caspase-3/GSDME axis in β-GP-induced calcification in MOVAS-1 cells, MOVAS-1 cells were stimulated by β-GP with si-caspase-3 or si-GSDME. First, the knockdown efficacy of caspase-3 and GSDME in MOVAS-1 cells was verified using the RT-PCR assay. Compared to β-GP+si-NC, caspase-3 was markedly downregulated in the β-GP+si-caspase-3 group, while the GSDME level was notably decreased in the β-GP+si-GSDME group (Figure 1A). As visualized by the Alizarin red staining assay, the percentage of calcification was sharply increased in β-GP-stimulated MOVAS-1 cells, which was markedly reduced by si-caspase-3 and si-GSDME (Figure 1B). The IL-1β level was found increased from 34.4 to 151.0 ng/L in β-GP-stimulated MOVAS-1 cells, which was reduced to 94.1 and 98.5 ng/L by si-caspase-3 and si-GSDME, respectively. Moreover, the IL-18 level in the control, β-GP, β-GP+si-caspase-3, and β-GP+si-GSDME groups was 92.5, 347.3, 221.2, and 216.3 ng/L, respectively (Figure 1C). The dramatically elevated LDH release observed in the β-GP group was markedly repressed by si-caspase-3 and si-GSDME (Figure 1D). Furthermore, the increased percentage of Hoechst-positive cells in β-GP-stimulated MOVAS-1 cells was notably reduced by si-caspase-3 and si-GSDME (Fig 1E). More importantly, levels of cleaved-caspase-3, GSDME-N, and NLRP3 were sharply increased in the β-GP group, which was markedly repressed by si-caspase-3 and si-GSDME (Figure 1F).

3.2. TMP alleviated the β-GP-induced calcification in MOVAS-1 cells

To explore the impact of TMP on β-GP-induced calcification in MOVAS-1 cells, MOVAS-1 cells were stimulated by β-GP, followed by treatment with 25 μM TMP for 24 h. The increased percentage of calcification in β-GP-stimulated MOVAS-1 cells was suppressed by TMP (Figure 2A). Furthermore, the elevated ROS level in β-GP-stimulated MOVAS-1 cells was reduced by TMP (Figure 2B). The IL-1β level in the control, β-GP, and β-GP+TMP groups was 49.4, 139.1, and 100.0 ng/L, respectively. In addition, the IL-18 level was found increased from 68.3 to 230.7 ng/L in β-GP-stimulated MOVAS-1 cells, which was reduced to 157.2 ng/L by TMP (Figure 2C). LDH release in the control, β-GP, and β-GP+TMP groups was 0.67, 2.25, and 1.29 mM, respectively (Figure 2D). The increased percentage of Hoechst-positive cells in β-GP-stimulated MOVAS-1 cells was greatly reduced by TMP (Fig 2E). Moreover, cleaved-caspase-3, GSDME-N, and NLRP3 were markedly upregulated in the β-GP group, which were greatly downregulated by TMP (Figure 2F).

3.3. The influence of TMP on β-GP-induced calcification in MOVAS-1 cells was abolished by the activation of caspase-3

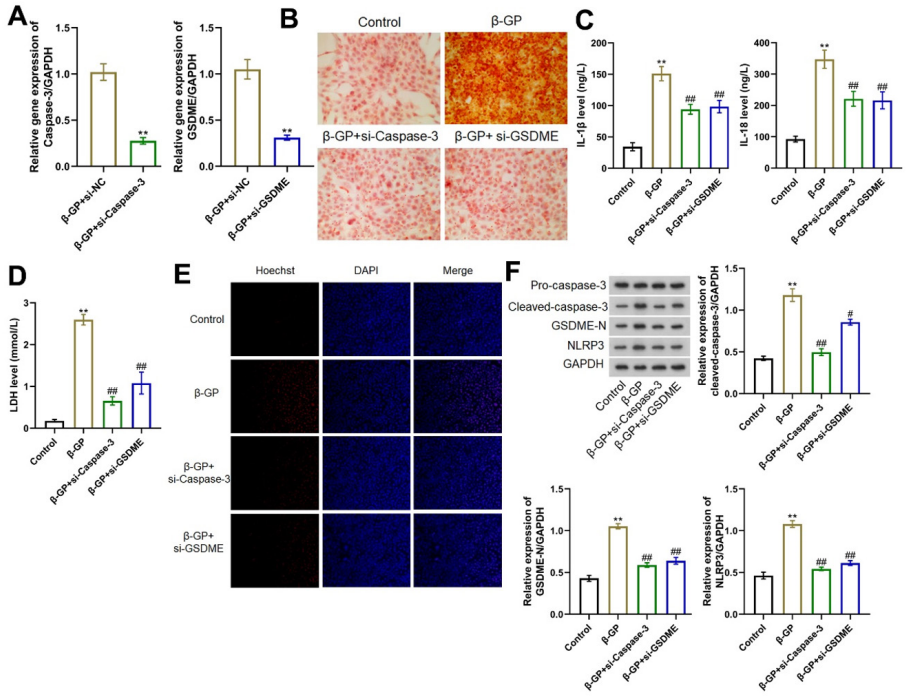

Figure 1. Caspase-3/GSDME axis was involved in β-GP-induced calcification in MOVAS-1 cells. (A) Knockdown efficacy of caspase-3 and GSDME in MOVAS-1 cells was verified using the RT-PCR assay (**$p < 0.01$ *vs.* β-GP+si-NC); **(B)** Calcification in MOVAS-1 cells was visualized using the Alizarin red staining assay; **(C)** ELISA assay was utilized for the detection of IL-1β and IL-18 levels in MOVAS-1 cells; **(D)** LDH release in MOVAS-1 cells was determined using a commercial kit; **(E)** Apoptosis of MOVAS-1 cells was evaluated using the Hoechst/PI staining assay; **(F)** Levels of cleaved-caspase-3, GSDME-N, and NLRP3 were detected using Western blotting (**$p < 0.01$ *vs.* Control, $^{\#\#}p < 0.01$ *vs.* β-GP).

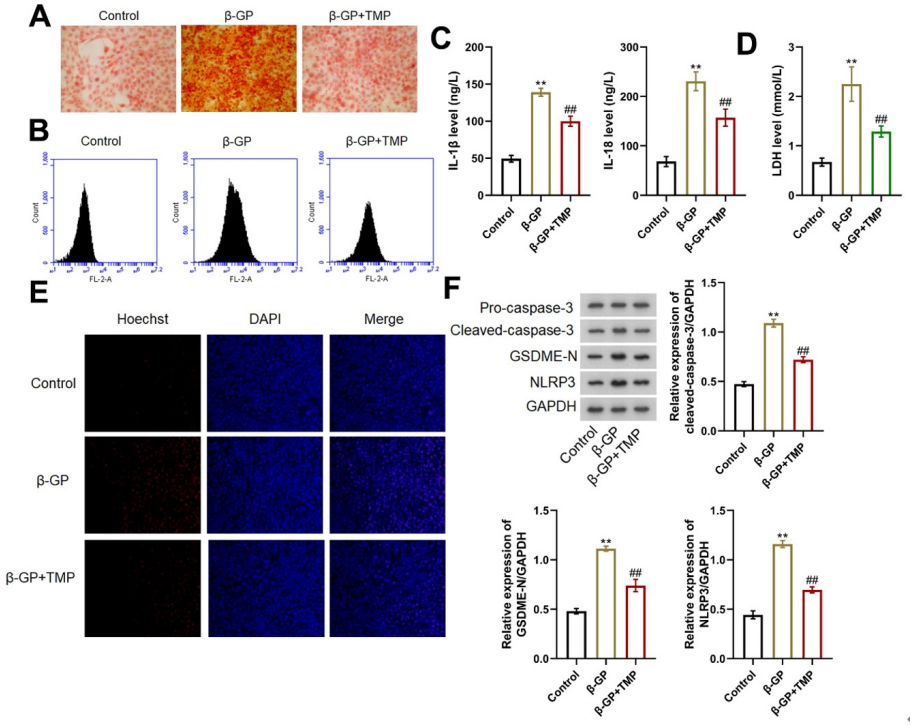

Figure 2. The β-GP-induced calcification in MOVAS-1 cells was alleviated by TMP. (A) Calcification in MOVAS-1 cells was determined using the Alizarin red staining assay; **(B)** ROS level was measured using flow cytometry; **(C)** ELISA assay was utilized for the detection of IL-1β and IL-18 levels; **(D)** LDH release in MOVAS-1 cells was detected using a commercial kit; **(E)** Apoptosis of MOVAS-1 cells was determined using the Hoechst/PI staining assay; **(F)** Expressions of cleaved-caspase-3, GSDME-N, and NLRP3 were detected using Western blotting (**$p < 0.01$ *vs.* Control, $^{\#\#}p < 0.01$ *vs.* β-GP).

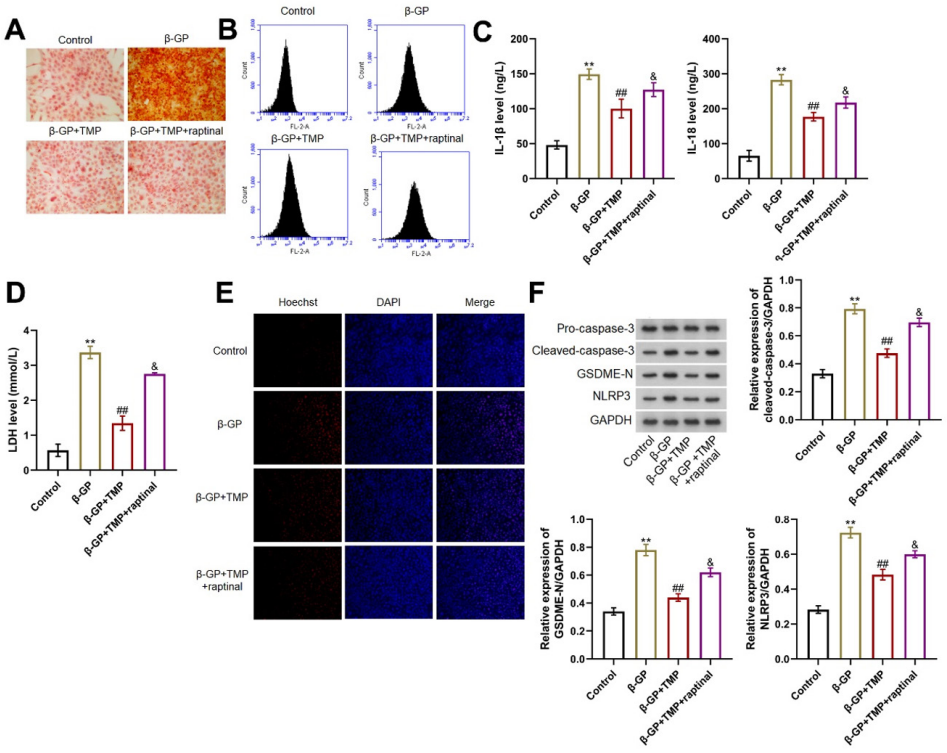

Figure 3. Activation of caspase-3 abolished the influence of TMP on the β-GP-induced calcification in MOVAS-1 cells. (A) Alizarin red staining assay was utilized to detect the calcification in MOVAS-1 cells; **(B)** Flow cytometry was used to measure the ROS level; **(C)** The IL-1β and IL-18 level in MOVAS-1 cells was determined by ELISA assay; **(D)** A commercial kit was used for the detection of LDH release in MOVAS-1 cells; **(E)** The Hoechst/PI staining assay was used for detecting the apoptosis of MOVAS-1 cells; **(F)** Western blotting was utilized to determine the cleaved-caspase-3, GSDME-N, and NLRP3 levels (**$p < 0.01$ *vs.* Control, $^{\#\#}p < 0.01$ *vs.* β-GP, $^{\&}p < 0.05$ *vs.* β-GP+TMP).

To identify whether TMP exerted anti-calcification function by inhibiting caspase-3, MOVAS-1 cells were stimulated by β-GP, followed by treatment with 25 μM TMP with or without 10 μM raptinal, an agonist of caspase-3. The increased percentage of calcification in β-GP-stimulated MOVAS-1 cells was reduced by TMP, which was elevated by the co-culture with raptinal (Figure 3A). Furthermore, the promoted ROS level observed in the β-GP group was decreased by TMP, which was reversed in the β-GP+TMP+ raptinal group (Figure 3B). IL-1β level in the control, β-GP, β-GP+TMP, and β-GP+TMP+ raptinal groups was 48.1, 149.2, 100.2, and 127.3 ng/L, respectively. IL-18 level in the control, β-GP, β-GP+TMP, and β-GP+TMP+ raptinal groups was 65.1, 282.6, 176.8, and 217.3 ng/L, respectively (Figure 3C). LDH release in MOVAS-1 cells was increased from 0.57 to 3.37 mM by β-GP, and was markedly reduced to 1.35 mM in the β-GP+TMP group, which was greatly reversed to 2.75 mM in the β-GP+TMP+ raptinal group (Figure 3D). The increased percentage of Hoechst-positive cells in the β-GP group was repressed by TMP, which was markedly reversed by the co-culture with raptinal (Figure 3E). Moreover, the elevated levels of cleaved-caspase-3, GSDME-N, and NLRP3 in β-GP-stimulated MOVAS-1 cells were notably reduced by TMP, which were markedly reversed in the β-GP+TMP+ raptinal group (Figure 3F).

3.4. TMP ameliorated the progression of CAC in OPG$^{-/-}$ mice

To identify the function of TMP against CAC, OPG$^{-/-}$ mice were used to mimic the clinical symptom of CAC, which were orally administered with TMP. Calcium deposition was obviously observed in OPG$^{-/-}$ mice, which was markedly alleviated by TMP (Figure 4A). Moreover, HE staining showed that the number of nodules was markedly increased in the model group, which was sharply reduced by TMP (Figure 4B). In coronary artery tissues, the IL-1β level was sharply increased from 44.1 to 142.4 ng/L in OPG$^{-/-}$ mice, which was greatly repressed to 77.1 ng/L by TMP. The IL-18 level in the control, model, and TMP groups was 52.8, 180.7, and 112.5 ng/L, respectively (Figure 4C). Increased levels of cleaved-caspase-3, GSDME-N, and NLRP3 in OPG$^{-/-}$ mice were markedly decreased by TMP (Figure 4D). Moreover, the upregulated CASP3 and ACTA2 in OPG$^{-/-}$ mice were downregulated by TMP (Figure 4E).

3.5. Inhibition of TMP on progression of CAC in OPG$^{-/-}$ mice was abolished by activation of caspase-3

To identify whether TMP exerted anti-CAC function by suppressing caspase-3, OPG$^{-/-}$ mice were administered TMP with or without raptinal, an agonist of caspase-3. The increased calcium deposition (Figure 5A) and

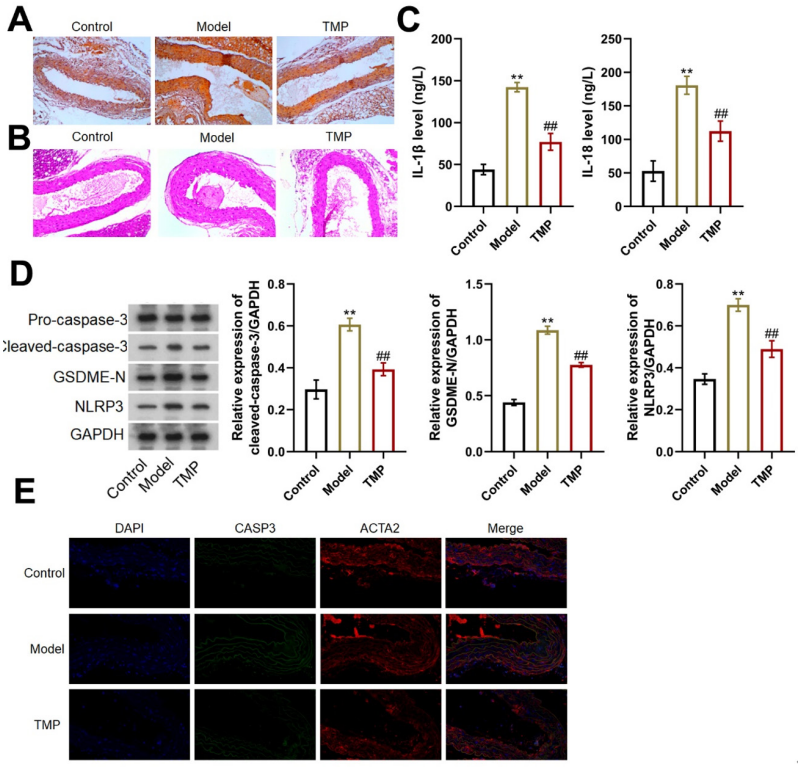

Figure 4. Progression of CAC in OPG$^{-/-}$ mice was ameliorated by TMP. (A) Calcification in coronary artery tissues was evaluated using the Von Kossa staining assay; **(B)** The pathological state in coronary artery tissues was evaluated using HE staining; **(C)** The IL-1β and IL-18 level in coronary artery tissues was detected using ELISA; **(D)** Expressions of cleaved-caspase-3, GSDME-N, and NLRP3 in coronary artery tissues were detected using Western blotting (**$p < 0.01$ *vs*. Control, $^{\#\#}p < 0.01$ *vs.* Model); **(E)** The expression of CASP3 and ACTA2 in coronary artery tissues was evaluated by immunofluorescence.

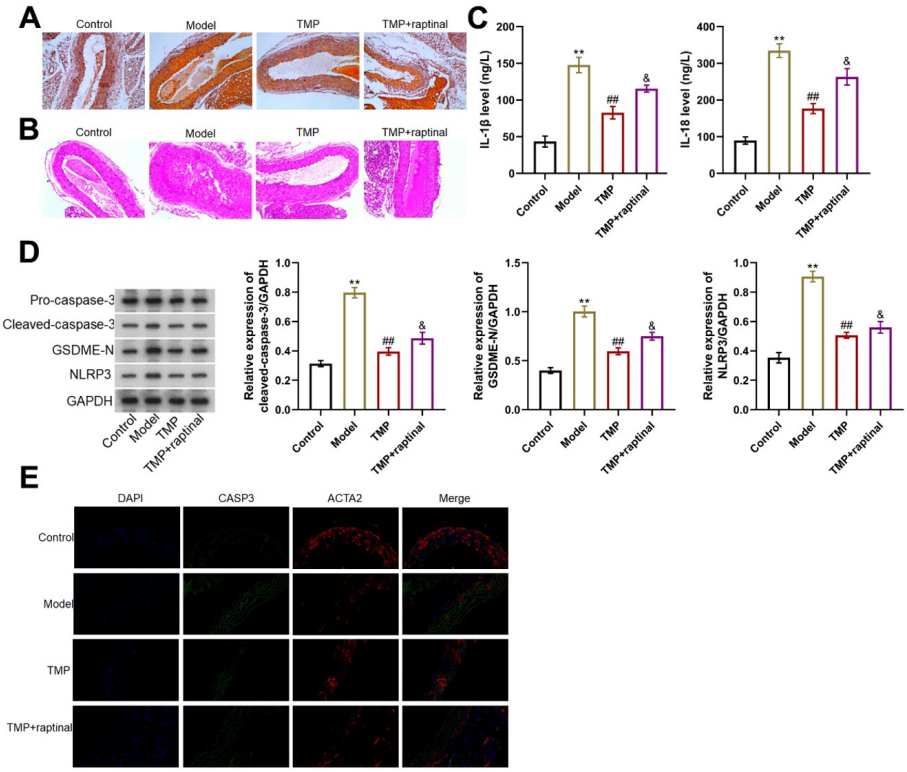

Figure 5. Activation of caspase-3 abolished the inhibition of TMP on the progression of CAC in OPG$^{-/-}$ mice. (A) Calcification in coronary artery tissues was determined using the Von Kossa staining assay; **(B)** HE staining was used to evaluate the pathological state in coronary artery tissues; **(C)** The IL-1β and IL-18 level in coronary artery tissues was measured using ELISA; **(D)** Western blotting was utilized to determine the cleaved-caspase-3, GSDME-N, and NLRP3 levels in coronary artery tissues (**$p < 0.01$ *vs*. Control, $^{\#\#}p < 0.01$ *vs*. Model, $^{\&}p < 0.05$ *vs*. TMP); **(E)** Expression of CASP3 and ACTA2 in coronary artery tissues was determined using immunofluorescence.

elevated number of nodules (Figure 5B) observed in OPG$^{-/-}$ mice were markedly repressed by TMP, which were signally reversed by the co-administration of raptinal. The IL-1β level in the control, model, TMP, and TMP+ raptinal groups was 43.5, 147.8, 82.7, and 115.5 ng/L, respectively. The IL-18 level in the control, model, TMP, and TMP+ raptinal groups was 89.6, 334.6, 176.8, and 263.2 ng/L, respectively (Figure 5C). The elevated cleaved-caspase-3, GSDME-N, and NLRP3 levels in OPG$^{-/-}$ mice were markedly reduced by TMP, which were sharply increased by the co-administration of raptinal (Figure 5D). The upregulated CASP3 and ACTA2 in OPG$^{-/-}$ mice were downregulated by TMP, the expression of which was notably increased in the TMP+ raptinal group (Figure 5E).

4. Discussion

Pyroptosis is a newly discovered cell death mode with a high degree of inflammation in recent years, which is programmed and controlled with the dual characteristics of necrosis and apoptosis, and finally triggers a secondary inflammatory response (*30*). Originally misclassified as apoptosis, pyroptosis was subsequently found to be a form of programmed cell death dependent on the Caspase family and mediated by the Gasdermin protein (*31*). Herein, as described in other research (*11,32*), β-GP was used to induce calcification in VSMCs, which was verified by increased calcification, enhanced inflammation, promoted LDH release, and aggravated apoptosis, accompanied by an activation of casaspe-3/GSDME signaling. Furthermore, these pathological changes in β-GP-stimulated VSMCs were sharply alleviated by the knockdown of casaspe-3 or GSDME, implying that caspase-3/GSDME axis mediated pyroptosis might participate in the progression of calcification in β-GP-stimulated VSMCs.

The present study investigates the molecular mechanisms underlying the protective effects of tetramethylpyrazine (TMP) on β-glycerophosphate (β-GP)-induced calcification and inflammation in MOVAS-1 cells and OPG$^{-/-}$ mice. The findings reveal that TMP significantly mitigates various pathological processes induced by β-GP, including increased calcification, elevated levels of reactive oxygen species (ROS), inflammatory cytokines such as Interleukin-1beta (IL-1β) and Interleukin-18 (IL-18), lactate dehydrogenase (LDH) release, enhanced apoptosis, and the activation of caspase-3/GSDME signaling. These effects were further corroborated *in vivo*, where TMP administration in OPG$^{-/-}$ mice significantly reduced calcium deposition and inflammation, effects that were reversed by raptinal, a caspase-3 activator. In addition, the increased calcification observed in β-GP-stimulated MOVAS-1 cells highlights the pro-osteogenic environment created by β-GP, a well-known calcification inducer. The concurrent elevation in ROS levels indicates oxidative stress as a critical mediator of this process. ROS are known to exacerbate vascular calcification by promoting the differentiation of vascular smooth muscle cells (VSMCs) into osteoblast-like cells. TMP's ability to reduce ROS levels suggests that it may exert its protective effects through antioxidant properties, thus preventing oxidative damage that contributes to calcification.

Inflammatory cytokines such as IL-1β and IL-18 play pivotal roles in vascular inflammation and calcification. The significant reduction of these cytokines by TMP treatment indicates its potent anti-inflammatory effects. This reduction may be attributed to the suppression of the NF-κB signaling pathway, which is a central regulator of inflammation. By inhibiting this pathway, TMP likely decreases the transcription of pro-inflammatory genes, thereby reducing the levels of IL-1β and IL-18.

The enhanced apoptosis and LDH release in β-GP-stimulated MOVAS-1 cells indicate cellular injury and membrane damage. LDH is a marker of cell membrane integrity, and its release signifies cell death. TMP's ability to attenuate these effects suggests that it may enhance cell survival by inhibiting apoptotic pathways. The involvement of caspase-3 in apoptosis is well-documented, and TMP's inhibitory effect on caspase-3 activation further supports its role in promoting cell survival. Pyroptosis, a form of programmed cell death distinct from apoptosis, involves activation of caspase-3 and GSDME. This study shows that TMP mitigates β-GP-induced pyroptosis by inhibiting the caspase-3/GSDME pathway. This inhibition is crucial, as pyroptosis contributes to inflammatory responses and calcification. The reversal of TMP's protective effects by raptinal, a caspase-3 activator, underscores the central role of caspase-3 in this process. Thus, TMP's ability to prevent pyroptosis may be a key mechanism through which it exerts its protective effects.

In OPG$^{-/-}$ mice, TMP administration significantly alleviated calcium deposition and reduced the number of calcified nodules. This model is particularly relevant as OPG deficiency is associated with increased vascular calcification, mimicking clinical conditions of enhanced calcification risk. The observed reductions in IL-1β and IL-18 levels, along with decreased expression of CASP3 and ACTA2, highlight TMP's broad anti-inflammatory and anti-calcification effects. Reversal of these protective effects by co-administration of raptinal further validates the role of caspase-3 in TMP's mechanism of action. The findings from the OPG$^{-/-}$ mouse model suggest that TMP may have significant therapeutic potential in treating vascular calcification and associated inflammatory conditions. By targeting multiple pathways involved in calcification, oxidative stress, and inflammation, TMP provides a comprehensive protective effect. This multi-target approach is advantageous in treating complex diseases like vascular calcification, where multiple pathological processes are involved. Herein, in line with

data presented by Osako (*33*), vascular calcification was observed in coronary artery tissues of $OPG^{-/-}$ mice, accompanied by enhanced inflammation and activated casaspe-3/GSDME signaling, which were also observed in β-GP-stimulated VSMCs. After administration of TMP, vascular calcification and inflammation were markedly alleviated, implying a promising anti-CAC property of TMP. The *in vivo* efficacy of TMP was in line with the observation in β-GP-stimulated VSMCs after the incubation with TMP, especially the repressive effect of TMP against the casaspe-3/GSDME signaling, suggesting that TMP might exert the anti-CAC property by inhibiting the casaspe-3/GSDME axis mediated VSMCs pyroptosis. Raptinal, the specific activator of caspase-3, was used to identify the function of casaspe-3/GSDME signaling in melanoma previously (*34*). Herein, suppressive effects of TMP on calcification in both β-GP-stimulated VSMCs and $OPG^{-/-}$ mice were abolished by raptinal, accompanied by enhanced inflammation and activated casaspe-3/GSDME signaling, suggesting that TMP exerted the anti-CAC function by inhibiting the casaspe-3/GSDME pathway. In future work, the relationship between the efficacy and doses of TMP will be explored to better support the therapy treating CAC using TMP. Collectively, TMP alleviated the progression of CAC by inhibiting caspase-3/GSDME mediated pyroptosis.

5. Conclusion

In summary, this study elucidates the protective mechanisms of TMP against β-GP-induced vascular calcification and inflammation. By inhibiting ROS production, reducing inflammatory cytokine release, preventing apoptosis, and blocking caspase-3/GSDME-mediated pyroptosis, TMP effectively mitigates the pathological processes associated with calcification. These findings provide a strong basis for further exploration of TMP as a therapeutic agent for vascular calcification and related inflammatory disorders. Future studies should focus on clinical trials to evaluate the efficacy and safety of TMP in human subjects, as well as exploring its potential synergistic effects with other therapeutic agents.

Funding: None.

Conflict of Interest: The authors have no conflicts of interest to disclose.

References

1. Soppert J, Lehrke M, Marx N, Jankowski J, Noels H. Lipoproteins and lipids in cardiovascular disease: From mechanistic insights to therapeutic targeting. Adv Drug Deliv Rev. 2020; 159:4-33.
2. Anzaki K, Kanda D, Ikeda Y, Takumi T, Tokushige A, Ohmure K, Sonoda T, Arikawa R, Ohishi M. Impact of malnutrition on prognosis and coronary artery calcification in patients with stable coronary artery disease. Curr Probl Cardiol. 2023; 48:101185.
3. Samadi S, Sadeghi M, Dashtbayaz RJ, Nezamdoost S, Mohammadpour AH, Jomehzadeh V. Prognostic role of osteoprotegerin and risk of coronary artery calcification: A systematic review and meta-analysis. Biomark Med. 2023; 17:171-180.
4. Kelly-Arnold A, Maldonado N, Laudier D, Aikawa E, Cardoso L, Weinbaum S. Revised microcalcification hypothesis for fibrous cap rupture in human coronary arteries. Proc Natl Acad Sci U S A. 2013; 110:10741-10746.
5. Narula N, Olin JW, Narula N. Pathologic disparities between peripheral artery disease and coronary artery disease. Arterioscler Thromb Vasc Biol. 2020; 40:1982-1989.
6. Opdebeeck B, D'Haese PC, Verhulst A. Molecular and cellular mechanisms that induce arterial calcification by indoxyl sulfate and p-cresyl sulfate. Toxins (Basel). 2020; 12:58.
7. Demola P, Ristalli F, Hamiti B, Meucci F, Di Mario C, Mattesini A. New advances in the treatment of severe coronary artery calcifications. Cardiol Clin. 2020; 38:619-627.
8. Henein M, Granasen G, Wiklund U, Schmermund A, Guerci A, Erbel R, Raggi P. High dose and long-term statin therapy accelerate coronary artery calcification. Int J Cardiol. 2015; 184:581-586.
9. Leopold JA. Vascular calcification: Mechanisms of vascular smooth muscle cell calcification. Trends Cardiovasc Med. 2015; 25:267-274.
10. Demer LL, Tintut Y. Inflammatory, metabolic, and genetic mechanisms of vascular calcification. Arterioscler Thromb Vasc Biol. 2014; 34:715-723.
11. Pang Q, Wang P, Pan Y, Dong X, Zhou T, Song X, Zhang A. Irisin protects against vascular calcification by activating autophagy and inhibiting NLRP3-mediated vascular smooth muscle cell pyroptosis in chronic kidney disease. Cell Death Dis. 2022; 13:283.
12. Wen C, Yang X, Yan Z, Zhao M, Yue X, Cheng X, Zheng Z, Guan K, Dou J, Xu T, Zhang Y, Song T, Wei C, Zhong H. Nalp3 inflammasome is activated and required for vascular smooth muscle cell calcification. Int J Cardiol. 2013; 168:2242-2247.
13. Wang Y, Gao W, Shi X, Ding J, Liu W, He H, Wang K, Shao F. Chemotherapy drugs induce pyroptosis through caspase-3 cleavage of a gasdermin. Nature. 2017; 547:99-103.
14. Shi J, Gao W, Shao F. Pyroptosis: Gasdermin-mediated programmed necrotic cell death. Trends Biochem Sci. 2017; 42:245-254.
15. Zhang Z, Zhang Y, Xia S, Kong Q, Li S, Liu X, Junqueira C, Meza-Sosa KF, Mok TMY, Ansara J, Sengupta S, Yao Y, Wu H, Lieberman J. Gasdermin E suppresses tumour growth by activating anti-tumour immunity. Nature. 2020; 579:415-420.
16. Jiang M, Qi L, Li L, Li Y. The caspase-3/GSDME signal pathway as a switch between apoptosis and pyroptosis in cancer. Cell Death Discov. 2020; 6:112.
17. Kayacan S, Sener LT, Melikoglu G, Kultur S, Albeniz I, Ozturk M. Induction of apoptosis by Centaurea nerimaniae extract in HeLa and MDA-MB-231 cells by a caspase-3 pathway. Biotech Histochem. 2018; 93:311-319.
18. Simonet WS, Lacey DL, Dunstan CR, *et al*.

Osteoprotegerin: A novel secreted protein involved in the regulation of bone density. Cell. 1997; 89:309-319.
19. Tsuda E, Goto M, Mochizuki S, Yano K, Kobayashi F, Morinaga T, Higashio K. Isolation of a novel cytokine from human fibroblasts that specifically inhibits osteoclastogenesis. Biochem Biophys Res Commun. 1997; 234:137-142.
20. Tan KB, Harrop J, Reddy M, Young P, Terrett J, Emery J, Moore G, Truneh A. Characterization of a novel TNF-like ligand and recently described TNF ligand and TNF receptor superfamily genes and their constitutive and inducible expression in hematopoietic and non-hematopoietic cells. Gene. 1997; 204:35-46.
21. Price PA, June HH, Buckley JR, Williamson MK. Osteoprotegerin inhibits artery calcification induced by warfarin and by vitamin D. Arterioscler Thromb Vasc Biol. 2001; 21:1610-1616.
22. Bucay N, Sarosi I, Dunstan CR, Morony S, Tarpley J, Capparelli C, Scully S, Tan HL, Xu W, Lacey DL, Boyle WJ, Simonet WS. Osteoprotegerin-deficient mice develop early onset osteoporosis and arterial calcification. Genes Dev. 1998; 12:1260-1268.
23. Min H, Morony S, Sarosi I, Dunstan CR, Capparelli C, Scully S, Van G, Kaufman S, Kostenuik PJ, Lacey DL, Boyle WJ, Simonet WS. Osteoprotegerin reverses osteoporosis by inhibiting endosteal osteoclasts and prevents vascular calcification by blocking a process resembling osteoclastogenesis. J Exp Med. 2000; 192:463-474.
24. Orita Y, Yamamoto H, Kohno N, Sugihara M, Honda H, Kawamata S, Mito S, Soe NN, Yoshizumi M. Role of osteoprotegerin in arterial calcification: Development of new animal model. Arterioscler Thromb Vasc Biol. 2007; 27:2058-2064.
25. Lin J, Wang Q, Zhou S, Xu S, Yao K. Tetramethylpyrazine: A review of its mechanisms and functions. Biomed Pharmacother. 2022; 150:113005.
26. Lu C, Jiang Y, Zhang F, Shao J, Wu L, Wu X, Lian N, Chen L, Jin H, Chen Q, Lu Y, Zheng S. Tetramethylpyrazine prevents ethanol-induced hepatocyte injury *via* activation of nuclear factor erythroid 2-related factor 2. Life Sci. 2015; 141:119-127.
27. Jiang F, Qian J, Chen S, Zhang W, Liu C. Ligustrazine improves atherosclerosis in rat *via* attenuation of oxidative stress. Pharm Biol. 2011; 49:856-863.
28. Jiang R, Xu J, Zhang Y, Zhu X, Liu J, Tan Y. Ligustrazine alleviates acute lung injury through suppressing pyroptosis and apoptosis of alveolar macrophages. Front Pharmacol. 2021; 12:680512.
29. Zhang F, Jin H, Wu L, Shao J, Wu X, Lu Y, Zheng S. Ligustrazine disrupts lipopolysaccharide-activated NLRP3 inflammasome pathway associated with inhibition of Toll-like receptor 4 in hepatocytes. Biomed Pharmacother. 2016; 78:204-209.
30. Yu P, Zhang X, Liu N, Tang L, Peng C, Chen X. Pyroptosis: Mechanisms and diseases. Signal Transduct Target Ther. 2021; 6:128.
31. Wang YY, Liu XL, Zhao R. Induction of pyroptosis and its implications in cancer management. Front Oncol. 2019; 9:971.
32. Ma WQ, Sun XJ, Wang Y, Zhu Y, Han XQ, Liu NF. Restoring mitochondrial biogenesis with metformin attenuates beta-GP-induced phenotypic transformation of VSMCs into an osteogenic phenotype *via* inhibition of PDK4/oxidative stress-mediated apoptosis. Mol Cell Endocrinol. 2019; 479:39-53.
33. Osako MK, Nakagami H, Shimamura M, Koriyama H, Nakagami F, Shimizu H, Miyake T, Yoshizumi M, Rakugi H, Morishita R. Cross-talk of receptor activator of nuclear factor-kappaB ligand signaling with renin-angiotensin system in vascular calcification. Arterioscler Thromb Vasc Biol 2013; 33:1287-1296.
34. Vernon M, Wilski NA, Kotas D, Cai W, Pomante D, Tiago M, Alnemri ES, Aplin AE. Raptinal induces gasdermin e-dependent pyroptosis in naive and therapy-resistant melanoma. Mol Cancer Res. 2022; 20:1811-1821.

Received April 15, 2024; Revised June 18, 2024; Accepted June 22, 2024.

**Address correspondence to:*
Honghui Yang, Department of Cardiology, Zhengzhou University, Central China Fuwai Hospital, No. 1, Fuwai Road, Zhengzhou 451464, China.
E-mail: 19503809999@163.com

Released online in J-STAGE as advance publication July 6, 2024.